A CRYOGENIC PLATFORM FOR SPACE BORNE INSTRUMENTS WITH NANOKELVIN STABILITY

W. Holmes[a], R. Bamford[a], T. C. P. Chui[a], J. Craig[b], S. Elliott[a], S. Galloway[b], J. Gannon[b], S. Park[b], P. Rentz[c], and J. Thomassen[b]

[a]Jet Propulsion Laboratory
California Institue of Technology
Pasadena, CA, 91109, USA

[b]Swales Aerospace
Pasadena, CA 91107, USA

[c]Logicon, Inc.
Montrose, CA 91110, USA

ABSTRACT

We describe the design and test of a modular 'probe' structure to allow nK control of <8kg space borne instruments operated at liquid helium temperatures for the Low Temperature Microgravity Physics Program. The probe consists of a 10" diameter plate on which is attached a 9.75" high 3 stage truss. This assembly is inserted into evacuated instrument space in a liquid helium cryostat. Germanium resistance thermometers with standard voltage readout and heater servo are used to control stages 1 and 2, the closest to the plate, to μK stability. Paramagnetic thermometers with DC SQUID readouts are used to control stage 3 to <1nK. A room temperature random vibration test at $7.7g_{rms}$ verified that the probe supports a 6.2kg mock instrument mounted on stage 3 under launch load for the Japanese HII-A rocket or the shuttle. The measured lateral stiffness is 1.8 MegaN/m. Thermal tests at T<7K show that for helium bath temperature drifts <0.1K, stage 3 can be maintained within 1nK from a temperature set point.

INTRODUCTION

The 'probe', shown in FIG 1, is a reusable, modular, cryogenic insert designed for fundamental physics experiments to be performed in space in the Low Temperature

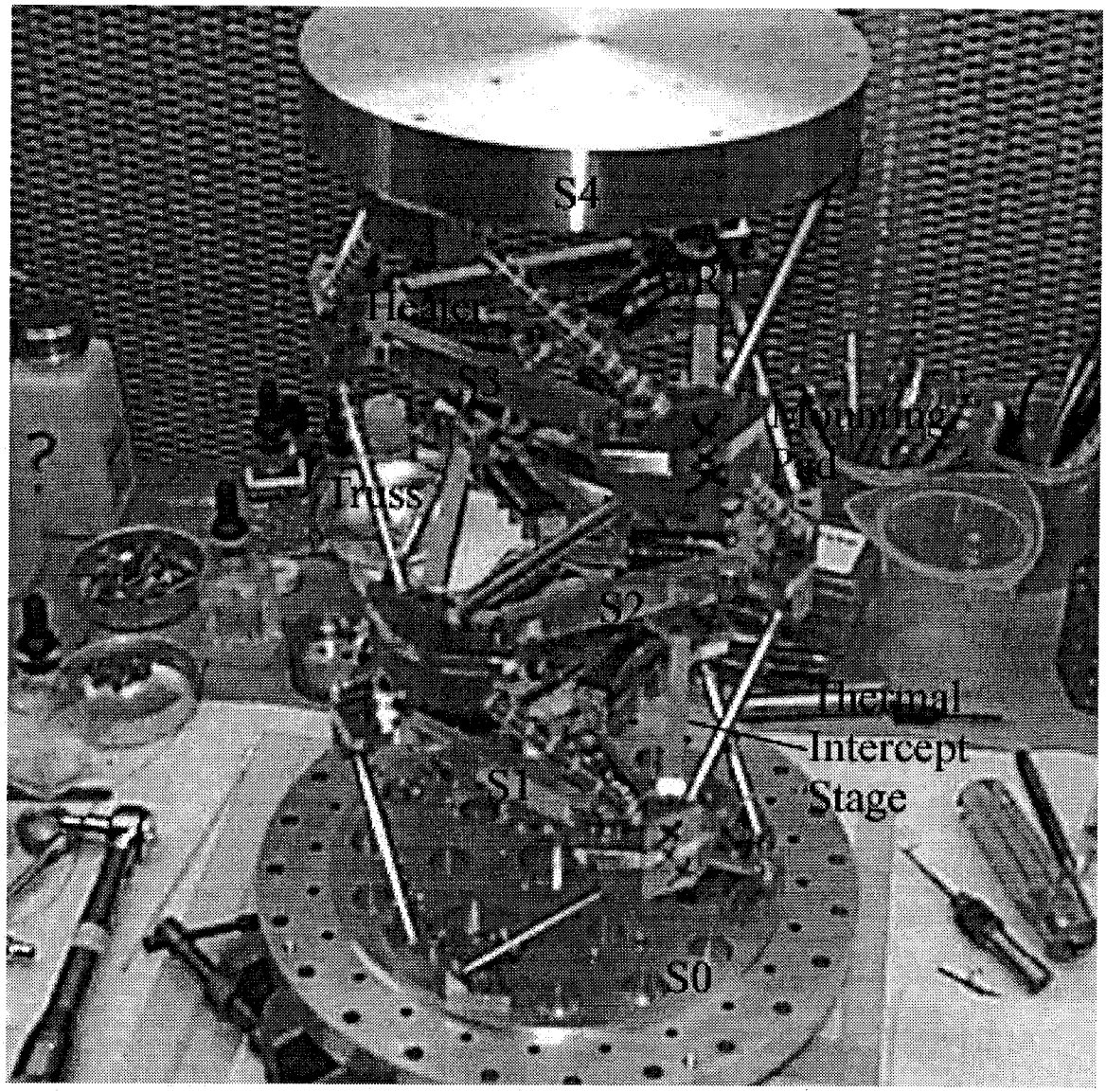

FIGURE 1. Picture of the prototype Probe truss. The fourth stage was removed for shake tests.

Microgravity Physics Facility (LTMPF).[1] Two tested experiment/probe assemblies will be installed onto the liquid helium tank of the LTPMF cryostat being developed at Ball Aerospace and Technology Corporation (BATC). The LTMPF cryostat is a major component of the facility. The cryostat, electronics boxes, and interface hardware are then integrated, tested, and shipped to the launch site. On orbit, LTMPF will be attached to the Japanese Experiment Module Exposed Facility. The 'probe' consists of a few components, a vacuum can, a mounting plate with hermetically sealed feedthrough flanges, a charcoal sorb pump,[2] DC SQUID magnetometers, and a thermally stabilized platform for the main experimental cell. The development and test of the thermally stabilized platform or 'probe truss' is the focus of this paper.

THERMOMECHANICAL DESIGN

The probe truss is required to enable nK control of experiments operated at liquid helium temperatures and to support hardware of mass up to 8kg during launch.

Stabilizing the temperature of a platform to sub-nK accuracy relies on the resolution of the thermometer and the dynamic range of the control circuit. Sub-nK temperature resolution has been achieved using a high resolution paramagnetic thermometer (HRT) readout with a SQUID magnetometer.[3,4] A total dynamic range $>10^8$ or >27 bits is required for the experiments using LTMPF. To achieve this, 3-4 stages, regulated with successively higher precision, are stacked. In this way, the dynamic range of the temperature control loop for each stage needed is ~1000, a value routinely achieved in the laboratory. Temperature stability, ~10μK, using germanium resistance thermometers (GRTs) is achieved on stages 1 and 2. Higher stability <10nK using HRT is achieved on stages 3 and 4. Temperature stability of ~1nK for the experimental cells used in the Lambda Point Experiment (LPE)[3] and the Confined Helium eXperiment (CHeX)[5] was realized on-orbit using this approach. The LPE/CHeX structure consisted of temperature regulated copper bus bars, brazed to pyramid-like arrangement of 3 stainless steel tubes. The mechanical strength was sufficient to support the <2kg LPE and CHeX experiment cells, but insufficient for the more massive experiments and higher launch loads anticipated for LTMPF. Furthermore, a higher degree of modularity was desired for experiments in LTMPF. This prompted a redesign of the probe truss.

The requirement for thermal stability is best expressed in terms of the isolation factor $F=\delta T_n / \delta T_{n+2}$. Here δT_n and δT_{n+2} are the temperature variations measured on stages n and n+2, where stage n+1 is regulated at a fixed temperature T_{n+1} between the temperatures T_n and T_{n+2} of stages n and n+2. A simple thermal model for 3 stages is shown in FIG 2. The temperature of S2 is only strictly controlled at the thermometer and follows the equation $(T_2- T'_2)Ga - C_tT_2/dt = P$, where P is applied power from the control heater. The small thermal conductance between the thermometer and the strut, Ga, and the small heat capacity of the thermometer, C_t, leads to small variations in the strut temperature T'_2 even if T_2 is perfectly controlled. The total heat flow through the strut obeys the relation, $-(T_3- T'_2)Gs + (T'_2- T_1)Gs - CdT'_2/dt = (T_2- T'_2)Ga$. Here T_1 is the temperature of S1, Gs is the thermal conductance of the inter-stage truss, and C' is the heat capacity of S2 minus that of the thermometer. When the parasitic power to S3 is negligible and the temperature of S3 is unregulated, the temperature T_3 of S3 follows $(T_3 - T_2)Gs - C_3dT_3/dt = 0$. The heat capacity of S3, C_3 is lumped since S3 is isothermal. We obtain the expression for $F=\delta T_3/\delta T_1 \sim (Ga/Gs + 1)(1-i2\pi f\tau)$, by propagating a disturbance on S1, $\delta T_1 \exp(i2\pi ft)$ oscillating at frequency, f, to S3 and dropping higher order terms in Gs/Ga. Here $\tau = C_2/ Gs$ is the bulk thermal time constant of the thermal intercept stage. At low frequencies, $f<<1/4\pi\tau$, or 'DC limit', the isolation factor is constant F~Ga/Gs. At high frequency, $f>>1/4\pi\tau$, F increases linearly with f, like the inverse of a single pole filter. Equivalently, the time dependence of a response in stage S3 to a step function change in T_1 is $\sim\exp(-t/\tau)$. For a stack of 4 stages, consider the response of S4 to the disturbance in S1 when both S2 and S3 are regulated. The stability of S4 is $\delta T_4=F(f)\ \delta T_2= F^2(f)\ \delta T_1$, when S2 and S3 are identical.

This 1D lumped element model is a very good approximation for temperature regulated platforms clamped at intervals along a single strut. The triangular platforms for LPE/CHeX and LTMPF can be reduced to the 1D model under the following conditions. The servo heat should be applied symmetrically, such as with 3 heaters placed near the support strut mounting pads, as shown in FIG 1 and thermal relaxation within the intercept stage is much faster than the control system and $\tau = C_2/Gs$. For materials such as pure annealed copper or aluminum and over the dimensions of a typical intercept stage, we estimate this internal relaxation time is <1ms. This is much faster than the control

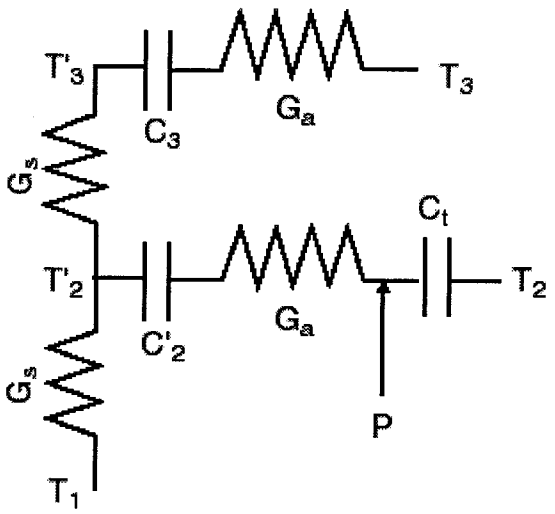

FIGURE 2. A simple thermal model of a three stage probe truss.

loop and τ. When the heaters are near each of the 3 mounting pads, the temperature measured with one thermometer on the thermal intercept next to one mounting pad is the same as the temperature near the other two mounting pads on the same thermal intercept. Therefore, Ga is determined by the distance of a single thermometer to the mounting pad. This approach for thermal control yields an improvement of a factor >10 over the standard approach of using only a single heater located next to the thermometer. A target value of F=1000, in the 'DC limit', was chosen so that the stability of a stage limited by the readout noise of a GRT is nulled to the nK level with only one stage. This value of F is also sufficient such that a stack of 3 stages with F=1000 nulls ~0.1K drifts in the cryogen temperature to <1nK at the third stage. Plugging this requirement into Equation (1) at f=0,

$$F \sim Ga/Gs = Ga\ l/NA\ \kappa_s > 1000, \qquad (1)$$

where κ_s is the thermal conductivity of the N inter-stage struts each of cross sectional area A and length l. Radiation coupling between stages is important only at the nK regulated stages. A radiation shield, not shown in FIG 1, surrounds successively more isolated stages.

The choice of material and the geometry of the inter-stage struts are also constrained by the total load on structure during launch. We performed a coupled loads analysis with launch loads defined at the carrier interface finite element models (FEM) of the CHeX cryostat and early models of the LTMPF cryostat to determine the launch acceleration needed to size the probe structure. We used an acceleration of a=40g, where $g=9.8 m/s^2$, for stress calculations. The strength of the LPE/CHeX structure was achieved by angling the support tubes to the center of mass of the experiment cells. Initially, we resized the support struts of the LPE/CHeX design to carry the larger loads expected for LTMPF experiments. In this design, a large fraction of the stress on the support struts at the base is due to bending which is structurally inefficient. Also, the position of the experiment mass is predetermined to be at the apex of the triangulated struts. If new experiments required a different geometry, the probe would have to be redesigned. We chose an alternative structure shown in FIG 1. Here, the inter-stage support is provided by 3 bipods which carry load predominantly in tension and compression, which is more structurally

efficient. Also, any number of stages can be stacked at the expense of lower load carrying ability. The maximum stress in any strut for a mass M on a 3 stage stack is

$$\sigma \sim 2.6 Mal/DA, \quad (2)$$

where D is the diameter of the intersection points of the bipods at each thermal intercept stage. The stress value in Equation (2) is the root square sum force for M accelerated simultaneously along each orthogonal axis. For the truss arrangement of the new design in FIG 1, the compressive and tensile stress dominate the bending stress in any strut. The maximum stress in any strut $1.5\sigma<\sigma_y$ must not exceed the yield stress σ_y for the strut material. The factor ~1.5 is a safety factor that accounts for variable values of σ_y and other imperfections in the material and fabrication process. For a given material, Equation (1) places a lower bound on l/A. Equation (2) and the requirement on maximum stress places an upper bound on l/A.

A final driving requirement for the design is the resonance frequency. This requirement is derived from several factors. The acceleration spectral density at the base of the truss, shown in FIG 3, is lower at frequencies higher than the cryogen tank resonances which were expected to be in the range 40-60Hz. If the resonant modes of the isolated cryogen tank and probe truss were too close, the modes would couple in the assembly and amplify the launch loads at the experiment. In addition, the vibrational energy during launch heats the cryogenic instrumentation[6] at a rate $P \sim 13.6 Ma^2_{PSD}$. Here, a^2_{PSD} is the acceleration power spectral density in g^2/Hz at the truss resonance frequency. Note that this rate is independent of the 'Q' of the resonance. The most effective way to minimize the vibrational power input at launch is to increase the truss resonance far from the cryostat resonances, where a^2_{PSD} is low. These factors set our minimum resonant frequency for the largest suspended mass to be ~1.5X frequency of the cryogen tank modes. We used a Finite Element Model (FEM) to determine mode frequencies for designs with different materials and sizes of the structural elements.

We chose a truss design made of 1/4" diameter rods of 304L stainless steel with an interstage height of 3.25" and diameter D=7.0" of the probe truss so that an average sized

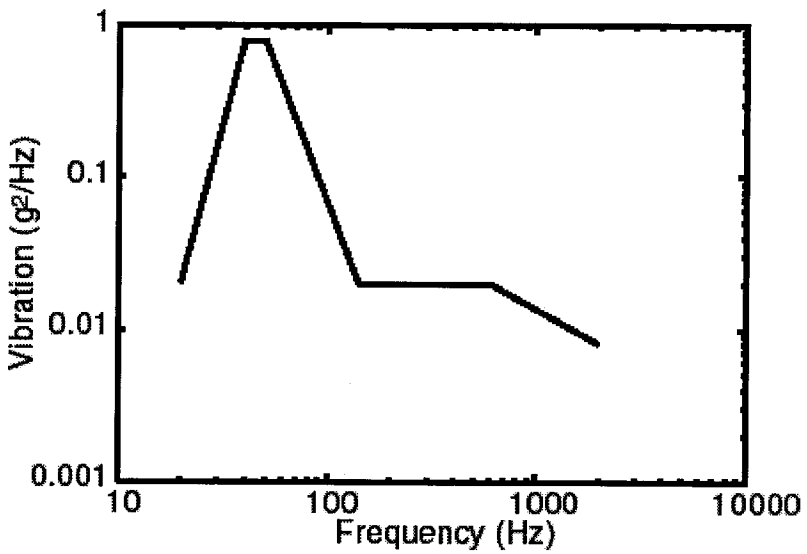

FIGURE 3. The acceleration power spectral density during launch at the attachment point of the LTMPF cryogenic inserts.

hand could fit between stages and down the axis of the 3 stage assembly. This design had sufficient strength for launch loads with suspended mass up to 6kg. Slightly larger, 5/16" diameter rods are required on the lowest stage for masses between 6 and 8kg. The corresponding thermal conductances are 0.16T and 0.25T mW/K respectively. Higher strength margins and isolation factors could be obtained using Ti6Al4V for the truss. However, the 304L SS truss satisfied requirements at a minimum cost. The cross sectional area of cross members for the triangular stages shown in FIG 1 was sized for maximum resonance frequency. The appropriately sized cross member of an aluminum intercept stage is ~ 0.3" by 0.5". A structure made of copper would have a smaller cross section ~ 0.25" by 0.4", but would be more than twice the mass of the aluminum stage. We calculated that the loads for the large 6-8kg mass experiments would yield the lowest stage if high thermal conductivity aluminum were used for a 3 stage stack. Therefore, for suspended mass of 6-8kg, a high strength aluminum alloy, 7075-T7 Al, is required on the lowest stage (S1) and pure, annealed aluminum, 1100-0 Al, can be used for the higher stages (S2 and S3). The values of G_a~750 T mW/K (40 T mW/K) were estimated for the Lakeshore GRT package[7] located a few millimeters from the truss mounting pad on 1100-0 Al (7075-T7 Al) intercept stages. The isolation factors for an assembly with 1/4" rods and an 1100-0 Al intercept (5/16" rods and an 7075-T7 Al intercept) is F=4600 (F=160). The low value of F for the latter, higher strength, inter-stage truss is acceptable when the first and second isolation stages (S1 and S2) are controlled using GRTs and the third (S3) is controlled using an HRT. The stacked combination of S1 and S2 gives a net isolation factor $F=7.4X10^5$ which nulls 0.1K variations to 140 nK which is within the range of control using an HRT.

Initially, the truss intercept joints consisted of two #6 and one #8 high strength A286 steel fasteners bolted into keenserts in the 1100 -0 Al intercept stage. A pair of 0.093" diameter steel pins at each joint carry shear load. The #6 fasteners attached from the topside and the #8 fastener attached from the bottom. A failure mode, shown in FIG 4, was found during the first random vibration test. This type of failure is not usually found in FEM models since a tensile load separates the interface between the pads and the intercept stage but a compressive load does not. There are three main design flaws. First, the bolts were initially sized using the maximum preloads for the high strength A286 #6

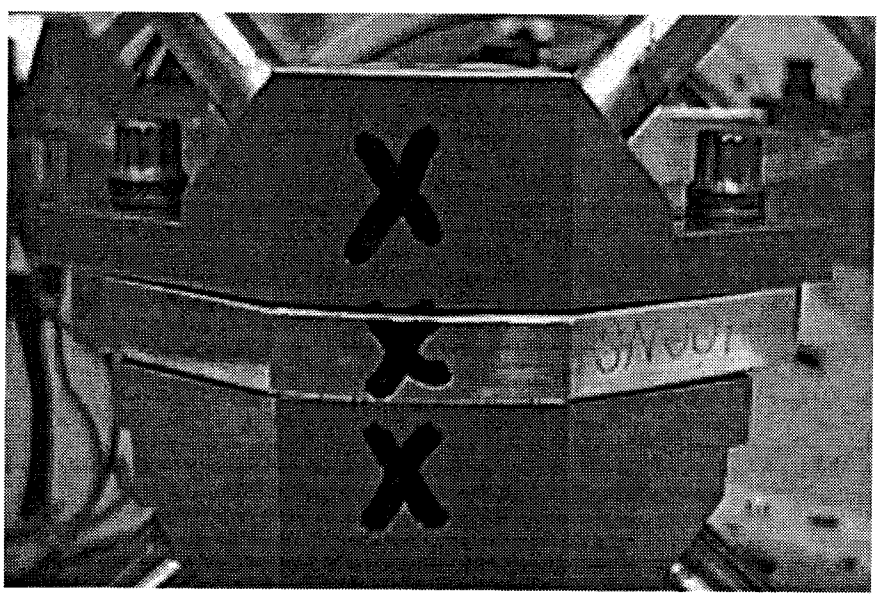

FIGURE 4. Failure of the first bolted joint design.

and #8 fasteners, 650 and 1100 lbs. respectively. The preloads for these fasteners in keenserts in 1100-0 aluminum, 71 and 184 lbs. respectively are limited by the shear strength of the aluminum threads. Second, when the load on the truss causes the interface to separate, the only contact points are at the edges of the pads, as shown in FIG 4. The fasteners and the force applied through the truss cause a torque about these edges. The fasteners have a smaller moment arm than the force applied through the truss. This mechanical "disadvantage" reduces the ability of the #6 fasteners to react the truss forces by a factor of ~4 per bolt. Third, the pin holes in the 1100-0 could not support the shear load. The pins were initially press fits in the aluminum. The pin holes were so severely deformed, the pins were loose and easily removed. In contrast to the damage on the intercept stages composed of 1100-0 Al, the keenserts and pin holes in the mounting plate, made of a high strength aluminum alloy, 6061-T6 Al, were undamaged. The redesigned joint on the prototype uses only a single #8. This fastener passes through the thermal intercept stage and bolts into a tap in the mounting pad of the adjacent truss. We did not modify the pin holes in the prototype. The flight design for the truss, currently in production, consists of 1/4" fasteners. The extra material, used for the #6 fasteners, was removed. The same 0.093" diameter steel pins are fit into 1/4" outer diameter 304 SS bushings press fit into the aluminum stage.

PROBE TRUSS FABRICATION

A prototype structure consisted of a brazed, 304L SS, interstage truss and aluminum intercept stages. The structure was mounted on a 6061-T6 Al plate for testing. For preliminary tests, interstage trusses made from 1/4" rod only were fabricated. The 1/4" rods were wiped with acetone and assembled into a set of 6 mounting pads in a fixture for brazing. The brazing compound, Palcusil 10, an alloy composed of 59% Ag, 31% Cu and 10% Pd, was used since it consists of non-magnetic materials. The assembly was brazed in a vacuum furnace at 1600 F for 6 minutes, cooled and held at 800 F for 1 hour and then cooled to room temperature. The joints were radiographically inspected to CWS 3.6 class A. Test coupons made from 304L SS stock rod with braze joints identical to those in the interstage truss were fabricated and pull tested. The measured yield strength for two test coupons was ~ 340 MPa. One braze joint separated at ~592 MPa. The other joint, which was not completely filled and did not pass inspection, released at a slightly smaller stress of ~510 MPa, but had the same yield strength.

Triangular stages made of 7075-T7351 Al and 1100-0 Al were fabricated. The 1100-0 Al thermal intercepts were machined from 1100-H14 Al plate, machined and then annealed to the -0 condition. The triangular plates were 1/4" thick at the bolted joint regions and tapered to a thicker 0.3" by 0.5" cross section between the bolted joint regions. These plates were easy to handle and suffered minimal damage during repeated assembly and disassembly. Triangular shape stages were a structurally sound choice, but constrained the volume on the inside of the probe truss. Circular stages offered a larger clear space on the inside of the truss for accessory hardware. Circular shaped stages were fabricated from 1100-H14 Al plate, machined and then annealed. These stages, which had a larger cross section than the trianglar stages, deformed quite easily when disassembled. Also, the probe truss with triangular intercepts had a measured resonance frequency that was about 10% larger than the assembly with all circular stages. The design with circular intercept plates was abandoned.

SHAKE TEST

We performed a total of 6 random vibration tests using the prototype probe structure with mass model instruments and several prototype science instruments. The tests were performed using a shake table at JPL. The shake system could apply an arbitrary random vibration spectrum using a reference accelerometer mounted on the shake table. The truss mounting plate was fastened to the shake table through force transducers. This allowed direct measurement of the force applied to the prototype and for force limited control.[8] Before each random vibration test, we verified the torque on all fasteners with a calibrated torque wrench. We performed a 1/4g amplitude sine sweep before and after the random vibration to determine if there was a structural failure. A sign of structural failure is a large percentage shift in the lowest resonance frequency measured in the sine sweep. We fit the mode frequencies, measured from the sine sweeps as a function M to the form for a simple 1D mass on a spring $4\pi^2f^2=k/(M+m)$. The effective spring stiffness, k=1.8MegaN/m and the amount of probe mass moving with M, m=0.14kg were determined from the fit. A low level test at about 10% the power of the random vibration spectrum in FIG 3 was performed as a system check and to confirm the expected force on the probe truss. Once we decided to go to a full level test, the vibration power was first applied at the low level and incremented by factors of 2 up to the full level. The full level random vibration was then applied for 1 minute. The probe truss was inspected after each full level test. Force limiting was used only for the largest mass, 6.2kg, tested at full level. We performed a sine sweep and random vibration test at ~3% full level with an 8kg suspended mass. We calculated that a full level test with the 8kg suspended load, even with force limiting, might yield the structure so we did not test further. None of the random vibration tests resulted in a significant frequency shift.

THERMAL TEST

After the shake test the probe was disassembled, inspected, and reassembled for thermal testing at liquid helium temperatures. A fourth stage was added to the top of the three stage assembly as shown in FIG 1 and bolted to the mounting plate. One GRT[7] was attached to each stage near a truss mounting pad. Three, 20 kOhm metal film resistive heaters epoxied into small aluminum blocks were mounted near each truss pad. The GRTs and heaters were heat sunk on each lower stage and wired to a 55pin hermetically sealed feedthrough on the mounting plate via twisted pairs of 0.005" diameter manganin with polyamide insulation. The manganin wires heat sinks were made by press fitting 1/4" diameter sapphire posts into aluminum block, wrapping the twisted pairs of wire around the posts, fixing the wires in place with GE varnish, and bolting the assembly to the stage. The resistance of a single wire between stages was <15 Ohms. An additional feedthrough was equipped with a VCR fitting to evacuate the insert. Activated charcoal was mounted, in good thermal contact to the mounting plate, to ensure a high vacuum when the insert was cooled to 4K. The remaining 16 feedthrough holes were capped with blank brass plugs. All feedthrough flanges and the main vacuum can flange were designed with a 'step seal' indium joint, sealed with 0.06" diameter indium wire. The mass of the prototype cryoinsert subassembly, with 45cm long vacuum can, mounting plate, feedthroughs, and 4 isolation stages with heat sinks is 9.5kg.

The GRTs were current biased with a square wave modulated at ~10 Hz. Each GRT voltage was monitored with a homemade preamplifier designed using commercial AMP01 chips which have ~10nV/rtHz voltage noise at 10 Hz. The preamplifer output voltage was digitized using a National Instruments AT-MIO-16X. The GRT resistance was calculated by comparison to the reference resistor, biased and amplified in the same manner as the GRTs, and converted to a temperature calibrations, accurate to ~1mK, to a NIST standard. The gain of the preamlifier was selected so that the Johnson noise voltage of the reference resistor, measured in a ~1kHz bandwidth, corresponded to 1 bit in the digitizer. The temperature was controlled using a software algorithm. Current to the control heater was output using a National Instruments AT-AO-6 card. We wrote the GRT measurement and temperature control software in LabView.

We facilitated a rapid cool of the probe structure to liquid helium temperature by back-filling the evacuated instrument guard vacuum with 10mL STP helium-4 gas. When the mounting plate cooled to 4K, the transfer gas was removed from the guard vacuum space by adsorption on to the activated charcoal.

We measured F for a truss with a high conductivity stage (S2) and a high strength stage (S3), shown in FIG 5 as follows. For S2, T_2 was regulated ~0.5-1K higher than T_1. Stages S3 and S4 were monitored, but unregulated. The temperature of S1 was increased by ~0.1-0.5K, and fixed until stages S3 and S4 equilibrated. Then T_1 was reset to the original value. We calculated $F=dT_3/dT_1$ from the data, where dT_3 was the maximum change in T_3 for the applied change dT_1. An identical technique was used to measure F for the high strength stage S3. Here, the temperature of S3 was fixed, S2 modulated, and the maximum change in S4 was measured. We measured F~7000 and F~2000, independent of temperature, for S2 and S3 respectively, in qualitative agreement with the model. In a separate test, when only one heater per stage was used, we measured F~ 400 validating our simple 1D model. The only disagreement with the model is that the measured values of F are higher than predicted.

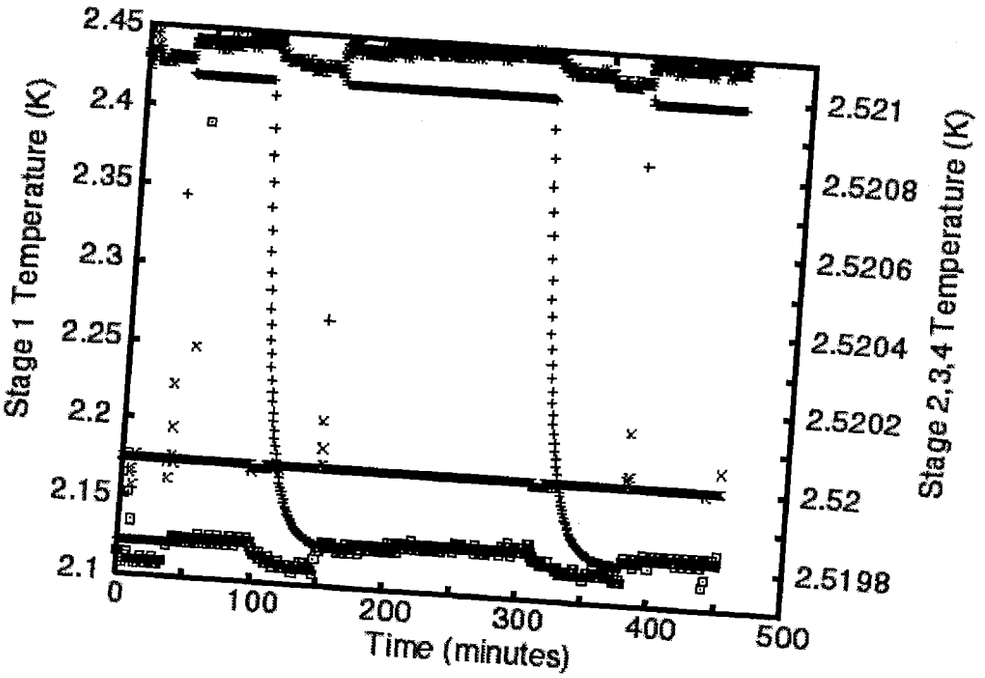

FIGURE 5. Typical measurement of F. The temperatures of S1(+) (S2 (X), S3(*) and S4 (squares)) are noted on the y-axis to the left (right). Temperature offset between S2, S3 and S4 are due to calibration error.

The temperature relaxation of S1 and S2 on cooling, shown in FIG 5, was fit to ~exp(-t/τ), to measure τ for S1 and S2. Similarly, we fit the time dependence of the temperatures of S3 and S4 after a sharp change in T_1 to calculate τ for these stages. The measured τ for all stages was between 12-14 minutes and independent of temperature. The heater power, P, required to maintain a fixed temperature gradient between stages was fit to the form $P=(NA\kappa_o/l)(T_{n+1}^2-T_n^2)/2$, to determine $Gs(T)= =(NA\kappa_o T/l)$. Here P applied to S2 varies to maintain a fixed temperature of S2, when the temperature of S1 changes. It is more common to fix the temperature of S1, apply power to S2 and measure the change in temperature of S2. We did not use the technique, since S3 and S4 would first have to equilibrate with S2. This would have taken at least 3 times longer. When heat applied only to S4, the temperatures of any two adjacent stages were consistent with the same κ_o for all inter-stage trusses. The value of κ_o ~1.2mW/cm-K^2 and temperature dependence agrees to 20% with published values for 304L SS.[9] The heat capacity of each stage, $C=\tau$ Gs~0.14 T J/K calculated from the measured τ and Gs is dominated by the stainless steel mounting pads.[10]

We attempted to measure F at lower temperatures <2K. When the stages cooled below the superfluid transition temperature, T=2.17K, F decreased to ~500. Both Gs and τ had the same value and temperature dependence as expected from measurements at higher temperatures. When all the stages were heated back to T>2.17K, we again measured F~7000 for S2. We suspect that this was due to a superfluid film from condensation of a small amount of the transfer gas causing a direct thermal short between non-adjacent stages. Since the data were taken over several days, and there was no change larger than 1% measured in the thermal conductance, it is hard to believe that superfluid leaked through any of the indium seals. We could test this hypothesis by repeating the measurements using a different transfer gas such as neon.

CONCLUSIONS

We have designed and tested a rugged, modular, truss structure to provide the ability to stabilize experiment temperature to a few nK for space borne experiments. Prototype truss hardware was subjected to several launch level random vibration tests with suspended masses ranging from 1-6.2kg and did not incur any structural damage. The main figure of merit for thermal performance, the isolation factor F, was measured over a range of temperatures 1.7 to 7K. The required value is F>1000. We measured F=7000 and F=2000 for assemblies with a thermal intercept stage made of pure annealed aluminum and high strength aluminum respectively. This exceeded our expectations. The design could be improved to support about twice the mass, to have slightly higher F and save about 0.6kg per 3 stage assembly by substituting aircraft grade titanium (Ti6Al4V) for the stainless steel parts in the current design. The probe truss will be used for experiments in the Low Temperature Microgravity Physics Facility to be berthed on the Japanese Experiment Module on the International Space Station.

ACKNOWLEDGEMENTS

We acknowledge Mark Weilert and other members of LTMPF science team for useful discussions and Christina Holmes for a extensive editting effort. The research described in this paper was carried out at the Jet Propulsion Laboratory, California

Institute of Technology, under a contract with the National Aeronautics and Space Administration.

REFERENCES

1. Larson, M., to be published in *Cryogenics*, (2001).
2. Lysek, M.J., et al., "Design and Testing of an Improved Cryopump for the Confined Helium Experiment," in *Advances in Cryogenic Engineering 43A*, edited by P. Kittel et al., Plenum, New York, 1998, pp. 995-1000.
3. Lipa, J.A, Swanson, D.R., Nissen, J.A., Chui, T.C.P., and Israelsson, U.E., *Phys. Rev. Lett.*, **76**, pp.944-947 (1996).
4. Welander, P., Hahn, I., and Barmatz, M., accepted for publication in *Rev. Sci. Instrum.*, (2001).
5. Qin, X., et al., *Cryogenics,* **36**, pp. 781-786 (1996).
6. McCammon, D., et al., *Nucl. Instrum. Methods*, **370**, pp. 266-268 (1996).
7. Lakeshore Cryotronics, 64 E. Walnut St., Westerville OH, Model GRT200A-2500-CD
8. Sharton, T., *Force Limited Vibration Testing Monograph*, Chapter 4, NASA Reference Publication RP-1403 (1997).
9. *Handbook on Materials for Superconducting Machinery*, 2nd Ed., Dept. of Defense, Metals Information Analysis Center, CINDAS/Purdue University, West Layayette, IN 46906, 1977, p. 8.1.2.7.
10. Hagmann, C. and Richards, P.L., *Cryogenics*, **34,** pp. 57-58 (1994).